Available online at www.sciencedirect.com
SCIENCE DIRECT®
Journal of Nuclear Materials 341 (2005) 189–200
journal of nuclear materials
www.elsevier.com/locate/jnucmat

Analysis of neutron attenuation in boron-alloyed stainless steel with neutron radiography and JEN-3 gauge

M. Bastürk [a,*], J. Arztmann [b], W. Jerlich [b], N. Kardjilov [c], E. Lehmann [d], M. Zawisky [a]

[a] TU-Vienna, Atomic Institute of the Austrian Universities, Stadionallee 2, A-1020 Vienna, Austria
[b] Böhler-Bleche GmbH, Mürzzuschlag, Austria
[c] Hahn-Meitner-Institute, Glienickerstraße 100 Berlin, Germany
[d] Paul Scherer Institute, Villigen, Switzerland

Received 28 October 2004; accepted 22 February 2005

Abstract

This paper concerns the neutron attenuation behavior of boron-alloyed stainless steels, and quantitative estimations of secondary effects on the neutron transmission measurements, such as beam hardening, background and micro-structure of neutron absorber causing a decrease in the total macroscopic cross-sections. Systematic thermal neutron transmission measurements of boron-alloyed steel plates have been performed at different neutron radiography facilities and at a portable gauge called JEN-3, which is a practical neutron transmission setup for industrial demands in non-destructive material inspection. In addition, MCNP (Monte Carlo Neutron Particle transport) simulations were performed for a better understanding of the experimental results, the secondary factors affecting the total macroscopic cross-sections, and the characteristics of the JEN-3 gauge. The detectable thickness limit for 1.88 wt% natural boron-alloyed steel plates was determined as 1–1.5 cm depending on the contributions of the secondary factors in each facility.

PACS: 24.10.Lx; 28.20.F; 29.27.Fh; 28.41.Pa; 29.40.Cs

1. Introduction

Boron is an important absorber used in neutron shielding materials like boron-alloyed steels to serve the storage of spent nuclear fuel, reactor shielding, nuclear waste disposals, Castor transport vessels and fuel shipment containers. Besides the beam attenuation characteristics of shielding materials, they have to be corrosion resistant under heavy duty. In Castor transport vessels, neutrons are slowed down to thermal energy by the interaction with moderator material (e.g. graphite or hydrogenous materials like water, paraffin, polyethylene) and then captured by the shielding materials like boron-alloyed steels for thermal neutrons, and lead, iron or concrete for gamma rays. Gamma rays are the most difficult to be shielded, and their attenuation process is a function of the atomic number and mass of the shielding material. On this account, materials with high atomic mass number and high

* Corresponding author. Tel.: +43 1 58801 14169; fax: +43 1 58801 14199.
E-mail address: bastuerk@ati.ac.at (M. Bastürk).

0022-3115/$ - see front matter © 2005 Elsevier B.V. All rights reserved.
doi:10.1016/j.jnucmat.2005.02.003

density like lead are used for gamma rays shielding. Because of the lower melting temperature of lead, medium weight element iron or concrete are used with the same mass as of lead where the temperature is high. Iron as stainless steel or carbon steel has been commonly used as the material for thermal shields. Such shield can absorb a considerable proportion of the energy of fast neutrons and gamma rays. However, this study focuses on the analysis of the thermal neutron beam attenuation by boron-alloyed steels, not gamma ray attenuation.

The distribution of absorbing elements within the shielding materials correlates with absorber content and material thickness in order to achieve specific beam attenuation. The absorption property of the boron-alloyed stainless steels depends solely on the content of the ^{10}B isotope within the natural or enriched boron-alloyed stainless steel. The ^{10}B-isotope has 3838.1 barn absorption cross-section for thermal neutrons [1]. Due to the high neutron absorption of boron compared to steel, the neutron radiography is a powerful tool for the non-destructive investigation [2]. The most important industrial demands for the shielding materials are the uniformity of the absorbing material over the whole volume and maximum thermal neutron absorption capability to perform the required safety functions. The type of the steel structure is a crucial factor to achieve a homogeneous distribution of borides in the steels. According to the type of steel, boron atoms concentrate on grain boundaries, or near grain boundaries [3]. Consequently, the definition of its neutron attenuation characteristics depending on the material thickness and density is of particular interest by applying the transmission technique.

The neutron attenuation of boron-alloyed austenitic stainless steels, where natural boron in the form of boron carbide is used, has been measured at two different thermal neutron radiography facilities, NR II (Neutron Radiography station II) at ATI-Vienna and NEUTRA (NEUTron RAdiography) at PSI. Neutron radiography (NR) is well-established as non-destructive material inspection method. In addition to the NR measurements, the same boron-alloyed steel plates have been measured by the JEN-3 gauge developed formerly by CEA (the French Atomic Energy Commission) for verifying the neutron attenuation in boron-alloyed stainless steel sheets or cladding materials. The JEN-3 is a portable, industrial, non-destructive material inspection setup and able to verify the attenuation of large steel sheets using neutrons, but it is not a radiography system [6]. Before starting with the neutron transmission measurements through boron-alloyed steels and quantitative estimation of the secondary factors, the principle and characteristics of the JEN-3 gauge was analyzed using MCNP simulations. The simulation of the JEN-3 gauge was motivated by the deviation of the measured total macroscopic cross-sections from the theoretically calculated values. The MCNP4b (4b version of the MCNP code) simulations of the JEN-3 gauge help better understanding of its working principle and optimization of its geometry if necessary. A set of MCNP studies have been generated, in which all interactions, system geometry, detector, materials and their cross-sections are described [5,6]. Briefly, this study covers the JEN-3 gauge analysis and estimation of some secondary effects on the neutron transmission measurements with different setups by comparing them with MCNP simulations.

2. Principle of the JEN-3 gauge

The JEN-3 gauge developed for verification of the boron in materials is utilized for routine testing of the neutron attenuation behavior of neutron shielding materials like boron-alloyed steel sheet (with a thickness $\leqslant 4.75$ mm) and plate (with a thickness $>$ 4.75 mm) in the Austrian fine steel production company 'Böhler-Bleche GmbH'. It is necessary to verify the effective boron content in the boron-alloyed stainless steel sheets. In this system, the absorbing sheet/plate to be checked is placed between a neutron source-detector block and a moderator and reflector as shown in Fig. 1. A small ^{252}Cf neutron source (3.5×10^6 neutron/s) and a half-cylinder ^3He counter are enclosed in a $20 \times 20 \times 20$ cm^3 steel box [6,7]. The ^3He counter with 3.7 cm diameter and 20 cm length is located 2 cm under the source in horizontal and vertical direction. In order to create a narrow detection angle, the horizontally placed ^3He counter is shielded with 0.2 cm thick Cd plates from the top and sidewise, which absorb thermal neutrons from undesirable directions. The second important part in this setup is the polyethylene desk of 5 m length, 1.3 m width, and 10 cm depth used as a neutron moderator [4,7]. The JEN-3 gauge is directly put on the samples on the polyethylene block with the help of a longer holder. Fast neutrons emitted from the ^{252}Cf source penetrate the polyethylene block after passing through the investigated material. The neutrons are moderated by the collisions mainly with ^1H and also ^{12}C atoms within the polyethylene block. The back-scattered thermalized neutrons are then attenuated by the sample. The detection efficiency of the ^3He neutron counter is maximal for thermal neutrons and negligible for fast neutrons. It is important point to be considered is that the area of the inspected sample should be larger than the detector acceptance window in order to count neutrons coming only from the sample, not from the surrounding polyethylene desk.

3. Simulations of the JEN-3 gauge

Prior to neutron transmission measurements through the boron-alloyed steel plates, a sequence of MCNP sim-

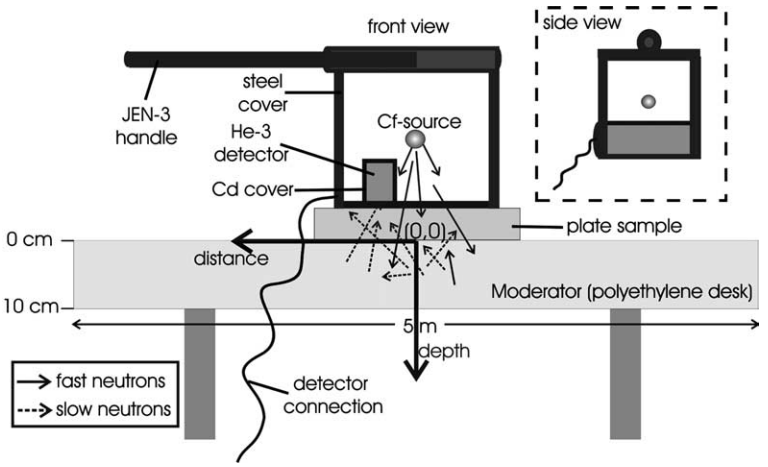

Fig. 1. Layout and principle of the JEN-3 neutron transmission gauge; the center on the polyethylene desk is chosen as the vertical projection of the Cf-source.

ulations were performed in order to analyze the JEN-3 gauge like neutron moderation within the polyethylene block, the distribution of thermal neutrons in the polyethylene moderator depth and on the moderator surface, and the detector response of the ^{3}He counter. The optimal distance between detector and sample was also studied in order to reduce the contribution of multiple scattered neutrons in the ^{3}He counter by increasing the distance. After the analysis of the JEN-3 gauge geometry, neutron transmission measurements were performed using 1.88 wt% natural boron-alloyed steel sheets. The absorption cross-sections of the ^{10}B isotope (natural boron contains 81.5 wt% ^{11}B and 18.5 wt% ^{10}B isotopes [8]) depend strongly on the neutron energy '1/v behavior' [1,9], which is included in the simulations.

3.1. Analysis of the neutron thermalization in the polyethylene moderator

The neutron moderation process in depth of the polyethylene block was analyzed so as to determine which neutron spectrum is relevant for neutron transmission measurements. The spectra were simulated at ten different points with 1 cm intervals in depth of the polyethylene. The simulated neutron spectra at 1 cm depth steps are shown in Fig. 2 where the maximum neutron intensity for thermal neutrons was found in the depth of 4–5 cm.

The distribution of the thermal neutrons in the moderator as a function of polyethylene depth was analyzed taking into account the integral of the thermal neutrons having energies up to 0.1 eV, see Fig. 3. The simulated total neutron flux decreases exponentially with increasing the polyethylene depth. At the end of the polyethylene moderator block (in 9–10 cm), the total neutrons decrease to 16% of the initial value because of neutron capturing and back-scattering processes. The maximum thermal-to-total neutron ratio was observed in the moderator depth of 7–8 cm. It can be concluded that a thickness of 10 cm of polyethylene desk is sufficient for neutron moderation and to achieve a proper thermal-to-total flux ratio in JEN-3 gauge. Only 5% of the total neutrons are available as thermal neutrons on the polyethylene surface for the transmission measurements.

3.2. Spatial distribution of the thermal neutrons on the polyethylene surface

The thermal neutron distribution on the polyethylene surface is simulated. The polyethylene surface is divided into tallies referring detector pixels to determine the most efficient area. The registered neutrons in each tally can be analyzed as a function of the distance from the center, which is the vertical projection of the Cf-source on the polyethylene surface. The real position of the ^{3}He counter is located 2–6 cm from that zero point shown in Fig. 1. The simulated open beam data (without sample) in Fig. 4 reveal an asymmetric thermal neutron distribution owing to the position of the neutron source at the sample position on the polyethylene surface where every point presents the detected neutrons in each detector tally. The neutron beam intensity decreases with the increasing distance from the vertical projection of the ^{252}Cf source on the surface; however, this problem should not affect the transmission result where the transmission is the division of each sample measurement by an open beam (without sample) value [7,10,11].

As mentioned before, the JEN-3 gauge is used for verifications of the shielding properties, especially boron-alloyed steel plates. On this account, we have used boron-alloyed steel plates as test samples in further MCNP simulations of the JEN-3 gauge. First,

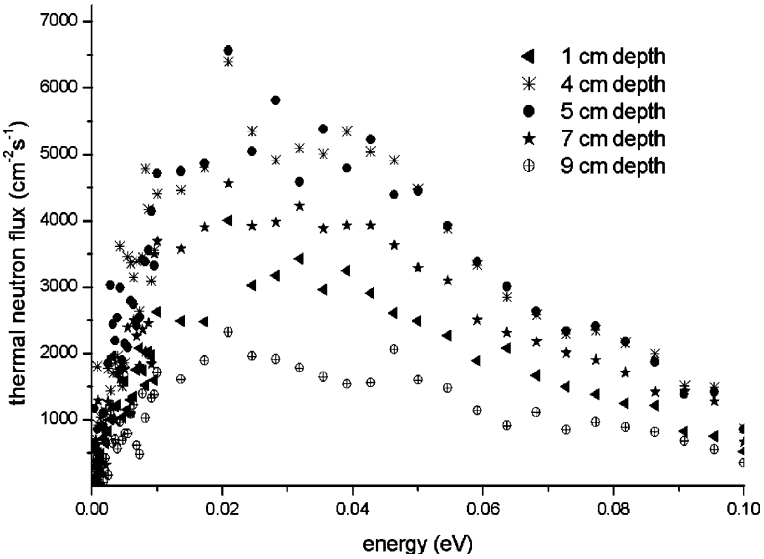

Fig. 2. Change of the neutron spectrum as a function of the polyethylene moderator depth: the thermal neutron spectrum is peaked around 0.02 eV. At depths larger than 5 cm, the thermal spectrum disappears owing to the back-scattered thermal neutrons.

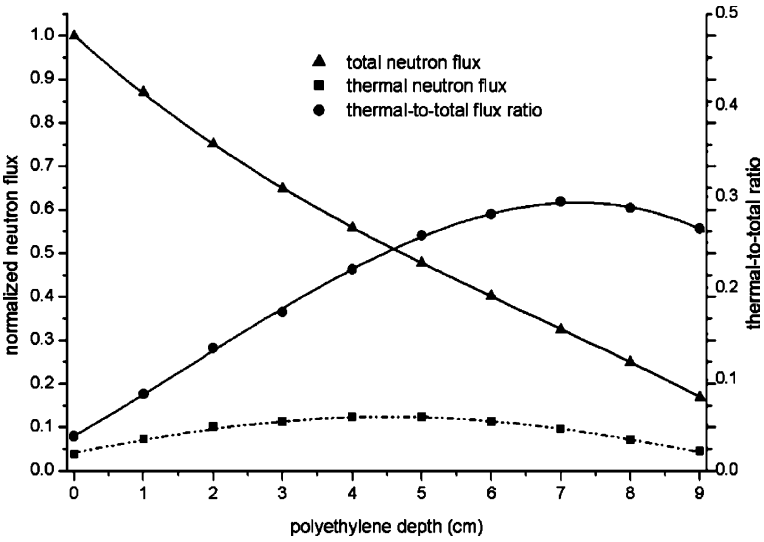

Fig. 3. Simulated total and thermalized neutron distributions as a function of the polyethylene depth (depth is indicated in Fig. 1). The maximal thermal neutron yield occurs at a depth of 5 cm, but the thermal-to-total ratio reaches its maximum at 7 cm.

the neutrons through a 0.55 cm thick 1.88 wt% natural boron-alloyed steel plate were simulated, and the output data were normalized by the simulated data without sample. Fig. 4 in logarithmic scaling reveals also a slight dependence of the neutron transmission on the distance (asymmetric neutron transmission), but this effect disappeared after the normalization. The actual ^{3}He counter position in JEN-3 gauge is also shown in Fig. 4.

3.3. Optimization of the detector–sample distance

One goal of this study is to analyze the contribution of the multiple scattered neutrons in the steel on the transmission results. Multiple scattered neutrons increase the neutron transmission in a short detector–sample configuration where the solid angle for detection of multiple scattered neutrons is larger. At an increased detector and sample distance, the multiple scattered neu-

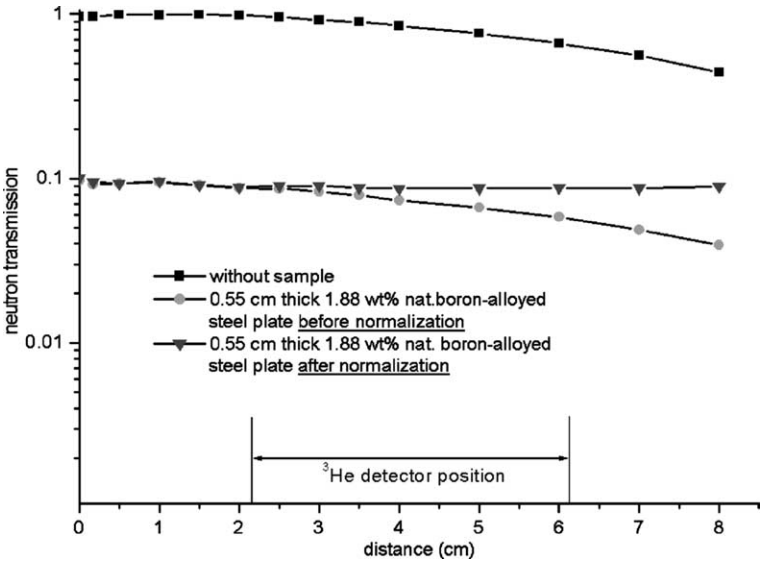

Fig. 4. The effect of the asymmetric neutron intensity distribution on the neutron transmission; neutron transmission through a 0.55 cm thick boron-alloyed steel plate on the polyethylene desk was simulated and then normalized with the open beam values without sample. The asymmetric intensity distribution is disappeared after normalization.

trons by the sample are scattered away from the detection area [7]. In order to show this effect, simulations were performed at different detector–sample distances. In the MCNP code, the registered neutrons can be classified as they were scattered before their detection or not, like total, transmitted and multiple scattered neutrons detected by the ^{3}He counter. This allows determining the contribution of the effect of multiple scattered neutrons on the transmission measurements. The distance of 5 mm between detector-sample in the actual JEN-3 gauge does not reduce the solid angle for multiple-scattered neutrons as schematically shown in Fig. 5 where most of detected neutrons consist of the multiple scattered neutrons by the sample.

The optimal distance between detector and sample could be determined to about 30 cm where the contribution of multiple-scattered neutrons (up to 1000 times scattered neutrons) is small enough, as shown in Fig. 6. Nevertheless, it manifests that the distance between detector and sample could not be increased because of

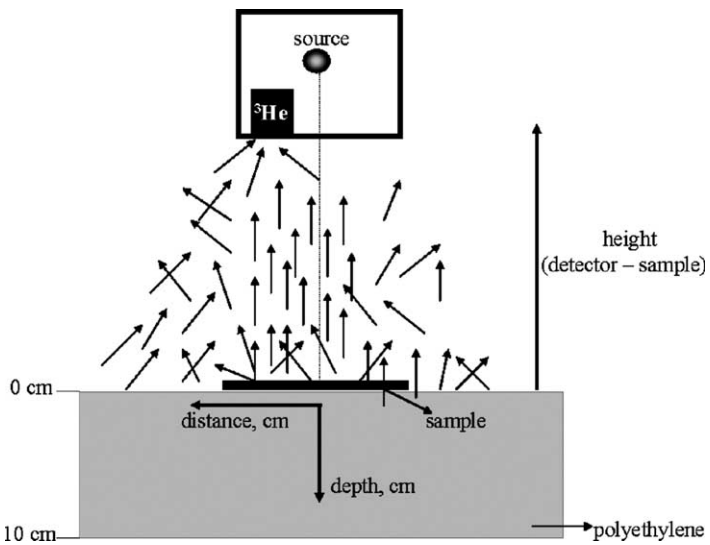

Fig. 5. A layout showing the optimization scheme for the detector–sample distance.

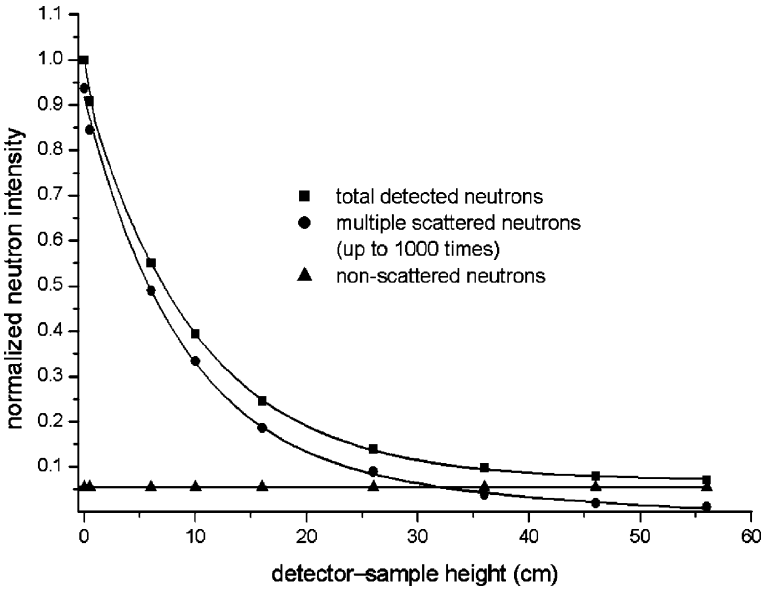

Fig. 6. Effect of the detector–sample distance variation on the neutron transmission through a 0.275 cm thick boron-alloyed steel sheet; an increment in distance between detector and sample causes an intensity decrease at the detector position, but the fraction of multiple scattered neutrons is largely reduced.

the decreasing intensity (detected total neutrons in Fig. 6). Furthermore, most of the detected neutrons at the increased detector–sample distance came from the polyethylene block, not through the sample. In these simulations, a 1.88 wt% boron-alloyed steel plate with a thickness of 0.275 cm was used. An optimization of the detector–sample distance in JEN-3 gauge is therefore not foreseen. As a result, the actual detector–sample distance of 5 mm was used in further simulations of the neutron transmission.

3.4. Simulation of the JEN-3 detector response

The detected neutrons in each tally can be simulated according to their energies defined in the energy card in the MCNP input file. In order to determine the detector response of the ^{3}He counter in the JEN-3 gauge, the detected neutrons on the polyethylene surface were analyzed according to their energies. To compare the JEN-3 detector response with the measured NEUTRA spectrum, the results were normalized as shown in Fig. 7 where the simulated JEN-3 response lies within the thermal energy interval. This proves that the ^{3}He counter recognizes the polyethylene desk as an isotropic source of thermal neutrons.

4. Measurements

The neutron transmissions through 1.88 wt% natural boron-alloyed stainless steel sheets (UNS S30467 – Type 304B7) were measured with the JEN-3 gauge and at two different NR facilities. The manufacture of the investigated boron-alloyed steel plates can shortly be summarized as following: Common austenitic steel is melted, and finally Ferro-boron is alloyed. The ^{10}B isotope in boron can be enriched, but in this article we focus on the natural boron composition. A specific rolling process is performed to achieve flat homogeneous steel plates, and thereafter, heat treatment is carried out in the form of solution annealing at a temperature of 1070 °C that is typical for austenitic steels. After sheet/plate finishing, the boron content is controlled wet chemically and with the JEN-3 gauge.

More than 20 plane-parallel boron-alloyed steel sheets were used in our neutron transmission measurements. One reference sheet of 0.0609 cm thickness was combined with 0.137 cm thick standard sheets in order to supply a small thickness increment. Due to the larger beam size and better beam characteristics, most neutron radiography experiments have been carried out at NEUTRA-PSI. The beam characteristics of both NR facilities, NEUTRA-PSI and NR II-ATI, are listed in the Table 1, more information can be found in [7,10].

The assessment of the neutron transmission and the total macroscopic neutron cross-sections using the JEN-3 data (counts) is easier than from NR images that require special filters to remove white spots on the images. The two-dimensional neutron transmission images were processed according to the digital image processing steps, as given in Eq. (1) where open (without sample) and dark (camera shutter closed) beam images

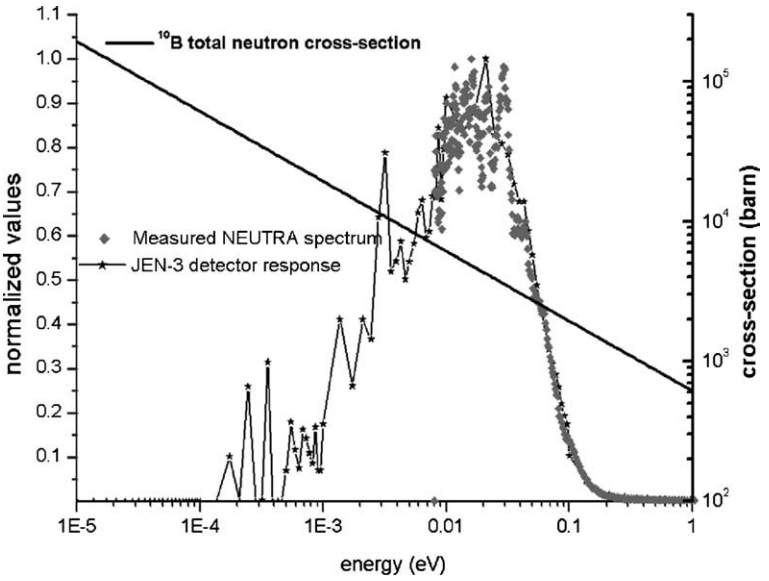

Fig. 7. Comparison of the JEN-3 detector response with the NEUTRA beam spectrum and the total neutron cross-section of ^{10}B isotope. The left axis shows the normalized values of the simulated JEN-3 detector response and the measured NEUTRA beam spectrum, and the right axis the total neutron cross-section of ^{10}B isotope as a function of neutron energy.

Table 1
Main characteristics of the neutron radiography facilities NR-II at the Atomic Institute-Vienna and NEUTRA at PSI-Villigen

	NR station-II ATI-Vienna	NEUTRA PSI
Neutron flux ($cm^{-2}\,s^{-1}$)	1.3×10^5	3×10^6
Collimation ratio	128	550
Cd-ratio	20	100
Beam diameter (cm)	9	40

are included. Open and dark beam corrections and normalization were applied to correct spatial fluctuations of the camera sensitivity as well as inhomogeneities of the scintillator and the neutron beam profile. Line profiles were taken on each transmission image at a specific position along the sample. The line profile gives quantitative information of the beam attenuation on its position on the radiography image [10,11]. The effective total macroscopic cross-sections were calculated from the neutron transmission through boron-alloyed stainless steel plates using Eq. (1) where $\Sigma_{B+Steel}$ and d are the macroscopic cross-section and the thickness of the boron-alloyed steel plate, respectively.

$$T=\frac{I_{sample}-I_{dark}}{I_{open}-I_{dark}}\cong\exp(-\Sigma_{B+Steel}\cdot d). \quad (1)$$

The expected macroscopic cross-section of homogeneous boron-alloyed steel containing 1.88 wt% natural boron was calculated as 7.32 cm^{-1} using the material cross-sections at thermal neutron energy [1]. The difference between measured data in different facilities given in Fig. 8 can be explained by the different energy spectra, background contributions, and other secondary effects like scintillator thickness at NR facilities, detector sensitivity, etc., peculiar for each facilities. The total macroscopic neutron cross-sections decrease with increasing the plate thickness of 1.88 wt% natural boron-alloyed steel. The background contributions related to the facility shown in Fig. 8 is explained in detail in Section 4.1.

The decrease of the effective total macroscopic cross-sections is due to background, beam hardening and absorber micro-structure; subsequently they can underestimate the neutron transmission and also lead to wrong results in the thickness calculation of the required shielding materials. In order to estimate the contributions of these individual factors, MCNP simulations have been performed in Section 5. From Fig. 8 it is obvious that shielding factors cannot be estimated from a simple exponential transmission law. Because applying such an idealized model is only valid if Σ_{eff} is constant at any depth.

4.1. Background factor

The neutron attenuation behavior for thicker 1.88 wt% natural boron-alloyed steel plates cannot be explained satisfactorily taking into account only the beam hardening and material heterogeneity factors. After a specific thickness, the measurements deviate from the simulations, which can be related also to the existence of some uniform neutron background in

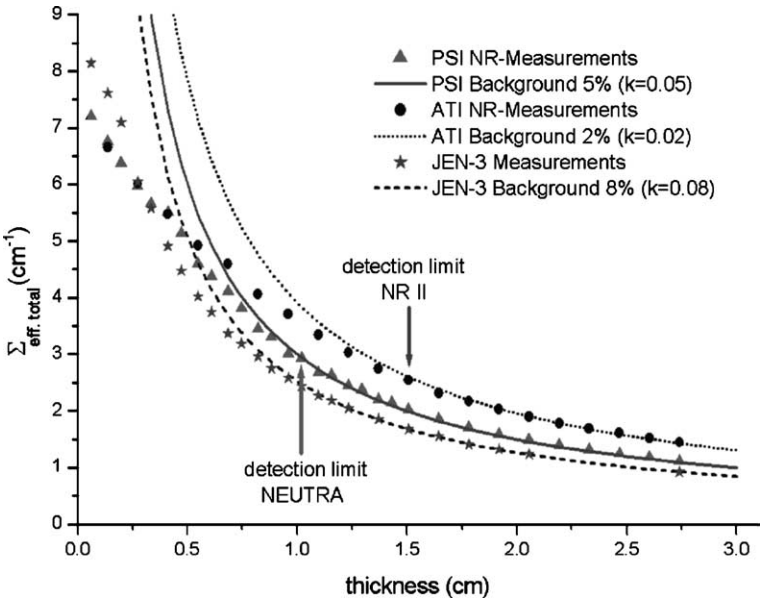

Fig. 8. Effective total macroscopic cross-sections of boron-alloyed steel plates as a function of material thickness measured with the facilities of NR-II, NEUTRA and the JEN-3. Background contribution at each facility was estimated; this factor dominates if the thickness approaches the detection limit.

the experimental facility. The sources for such a background are mainly scattered neutrons and detector specific noises like thermal, photon and readout noises. The constant background from the equipment is removed by the correction in Eq. (1). One can conclude from Fig. 8 that the background is accessible from measurements at higher thicknesses, where the signal from transmitted neutrons is negligible. The constant background in this case is dominant and the measured signal levels after this point cannot be explained with an MCNP model, where the background is not included. The only way to simulate background effects in MCNP is to define an excess uniform neutron source in the input file. Since we do not know the exact background level at the NR facilities, we cannot perform a reliable simulation. Instead of this, we tried to estimate the level of the background I_{BG} by the following assumption: if the investigated sample does not influence the spatial distribution of the background, then the background can be considered to be proportional to the initial beam intensity I_0 as in Eq. (2), where k is a proportional coefficient representing the background contribution factor of the facility [7,13]

$$I_{BG} = k \cdot I_0. \tag{2}$$

Consequently, using this assumption, Eq. (3) can be obtained for the experimental transmission where I_0 and I are the initial and the transmitted neutron intensities

$$\frac{I_{exp}}{I_{0,exp}} = \frac{I + k \cdot I_0}{I_0 + k \cdot I_0}. \tag{3}$$

For thicker absorbers the number of the transmitted neutrons will be very small ($I \approx 0$), which gives directly the boundary condition as stated in Eq. (4)

$$\frac{I_{exp}}{I_{0,exp}} = \frac{k}{1+k}, \quad \text{at } I \approx 0. \tag{4}$$

Therefore, the total macroscopic neutron cross-sections for a thick absorbing material where the transmitted neutron intensity is very small in comparison to the uniform background can be expressed as in Eq. (5) [13]

$$\Sigma(d) = -\frac{1}{d} \cdot \ln\left(\frac{k}{1+k}\right). \tag{5}$$

This assumption was applied to measured data, and rough background contributions in the JEN-3 and NR facilities were determined to 2% for NR II-ATI, 5% for NEUTRA-PSI, and 8% for JEN-3 by using the Eq. (5). In this case, a detection limit can be defined where the measured signal approaches the background level ($d_{max} \simeq 1.0$ cm for the JEN-3 and $1.0 < d < 1.5$ cm for the NR measurements).

5. Simulations of secondary effects on neutron transmission experiments

The transmission measurements were accompanied by MCNP simulations to verify the beam hardening effect and the micro-structure of Ferro-borides. The exponential decrease of simulated and measured total macroscopic neutron cross-sections as a function of

material thickness as seen in Fig. 8 is related to the well-known beam hardening effect [9]; however, the disagreement between expected and measured values is too large and requires other assumptions such as material microstructure and the neutron background.

5.1. Simulation of beam hardening

It has recently been verified that beam hardening in strong absorbing steel can cause strong deviations from the experimental transmission law [7,9,12]. This effect takes place in strong absorbing materials such as boron ($\sigma_a/\sigma_s \cong 200$ for thermal neutrons) where the absorption probability of slow neutrons increases inverse proportional with neutron velocity. Consequently, the mean energy of transmitted neutrons through such a material will be higher than before the penetration because of the preferred absorption of low-energy neutrons in the material [9,12]. The total macroscopic neutron cross-sections of ^{10}B isotope depend strongly on the neutron energy as shown in Fig. 7, where it is compared with the neutron energy spectrum of NEUTRA facility. The measured neutron energy spectrum of the neutron radiography beam line, NEUTRA, was used as an input spectrum into the MCNP code, and simulated output spectra have been analyzed behind different thicknesses of stacks of homogeneous boron-alloyed steel plates. The agreement between input and simulated output NEUTRA spectra without sample verifies the correct input geometry described in the MCNP simulations. The beam hardening caused by the absorber material itself is shown in Fig. 9 in logarithmic scaling. The emerging spectrum shift to the higher energy region with increasing material thickness shows that the absorber material causes a strong beam hardening effect, which appears as exponential decrease in the measured and simulated total macroscopic neutron cross-sections. That means the beam hardening effect was considered in both measured and simulated data.

5.2. Modeling the boron micro-structure

For material characterization it is of specific importance to define quantitatively the homogeneous distribution of strong absorbing elements within shielding materials. Till now, a homogeneous material structure was defined in the input files of MCNP simulations to show the influence of the beam hardening. If we compare the measured total macroscopic cross-sections with the MCNP simulations of the homogeneous boron distribution within the steel matrix, there is an evident deviation between them. As a result of this, further simulations were focused on the effect of the absorbers micro-structure. Firstly, one of the boron-alloyed sheets was investigated by SEM (scanning electron microscopy) [4] to determine the borides distribution in the sample. The SEM slice investigation of the 304B7 type boron-alloyed stainless steel shows the micro-structure of the borides in the metal matrix as shown in Fig. 10 (left image). The ideal case of a completely homogeneous boron distribution cannot be fulfilled in practice. Boron-alloyed stainless steels show excellent attenuation homogeneity on a macroscopic scale, but the microstructure is another source for the enhanced neutron

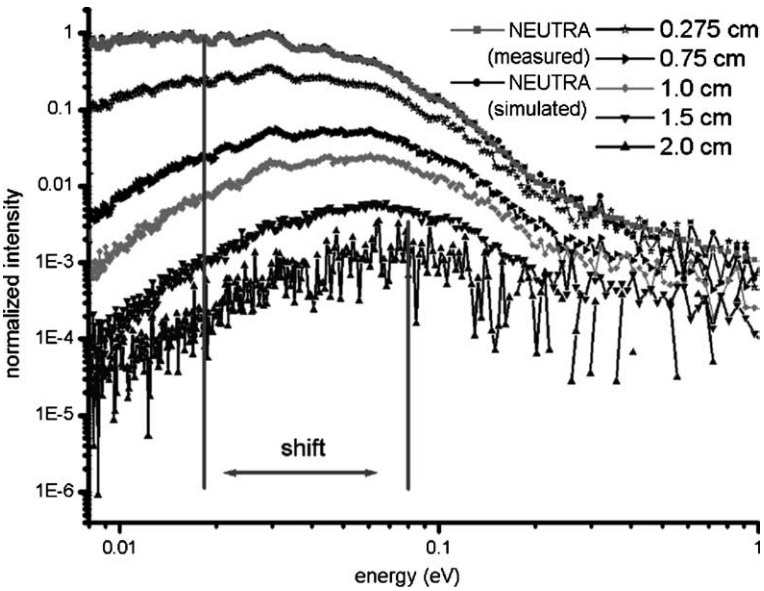

Fig. 9. Simulation of the beam hardening effect; the change of the neutron energy spectrum before and after the transmission through boron-alloyed steel plates with different material thicknesses reveals beam-hardening in the strong absorbing material.

transmission even if NR measurements of these sheets showed a perfect homogeneous structure. The NR image resolution was between 180 and 500 μm at NR II–ATI and this resolution cannot visualize if the material has really micro-scale structure. Although the Ferro-borides distribute randomly in each sample, the micro-structure within the sample was approximated by a simplified model. A two-phase model was used in the simulation to verify the effect of micro-structure on the neutron transmission as demonstrated in Fig. 10 (right image). The basis of our structural modeling is to provide a more realistic simulation of the transmission experiments. In this specific model, the homogeneous and inhomogeneous boron areas were ordered as a channel model. The borides distribution on the micro-scale was concentrated in one part of a unit cell keeping the total weight percent of natural boron constant in the sample. That means, the heterogeneous unit cell is composed of two homogeneous sub-cells, homogeneous steel and homogeneous boron-alloyed steel.

The size of the unit cell was taken 200 μm × 200 μm that is comparable with the spatial image resolution of NR measurements. A measure for the level of the sample homogeneity is the ratio between the volumes of both homogeneous parts in the unit cell. The size of sub-cells was varied and the best agreement between experiments and MCNP simulations was found at 18% heterogeneity as seen in Fig. 11 [7,13]. There are several possibilities to simulate geometrical structures; our model is probably the simplest one. Therefore, one has to be cautious,

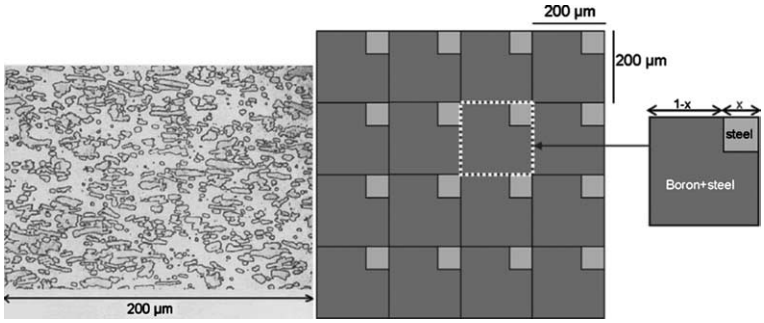

Fig. 10. SEM slice image shows the randomly distributed borides in a 304B7 type boron-alloyed stainless steel sheet (left image), and representation of the micro-structure used in the MCNP simulations (right image): the micro-structure level is defined by the ratio of the two homogeneous areas.

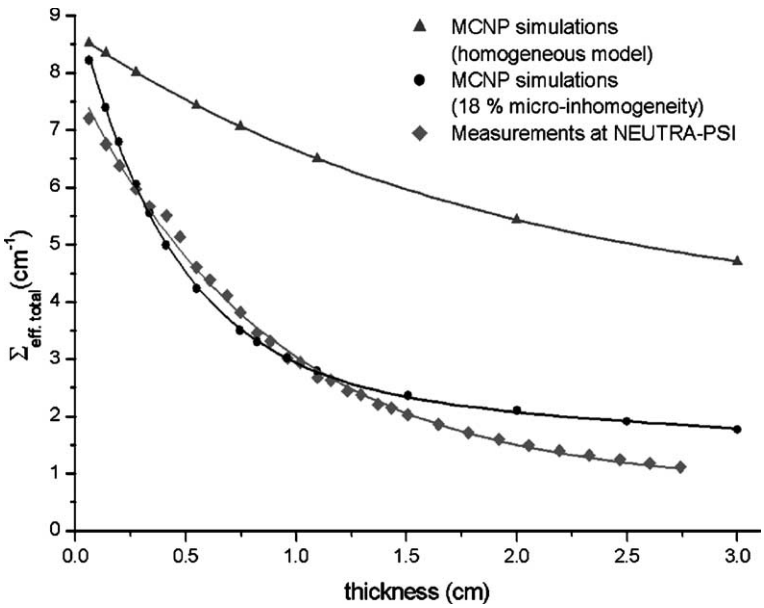

Fig. 11. Effect of micro-structure of the absorbing material on the neutron attenuation: the best agreement between measurements and simulations was achieved by using 18% micro-heterogeneity in the simulations.

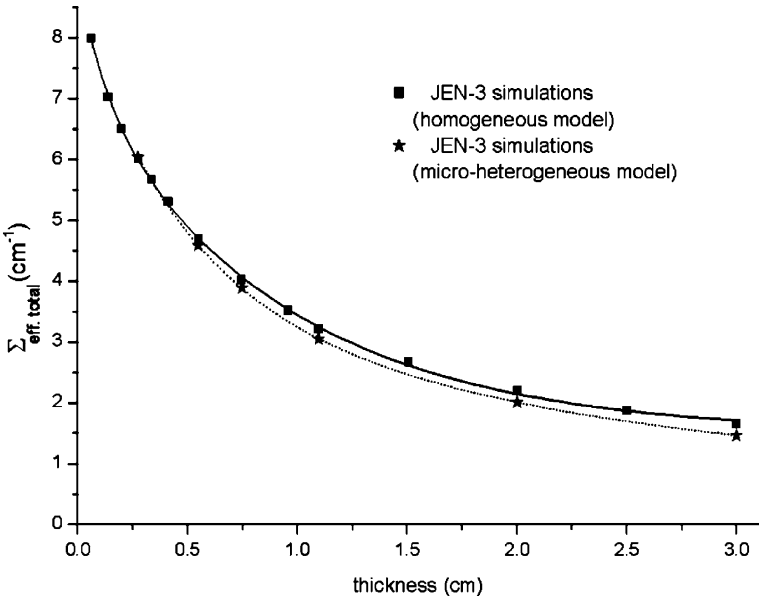

Fig. 12. Simulated sensitivity of the JEN-3 gauge to the micro-structure in boron-alloyed steel sheets: the borides micro-structure in the stainless steel sheet has no effect on the uncollimated neutron beam attenuation.

and certainly at the present stage it is not possible to consider our MCNP simulation as the true physical model. However, the more realistic random distribution of boron in the steel matrix was not available for a simulation.

The simple micro-structure model was also used in the JEN-3 simulations, and the results were compared with the simulations of homogeneous material structure. The purpose of these simulations is to determine if the setup is sensitive for micro-heterogeneities in the shielding materials. The contribution of multiple scattered neutrons is dominant in the neutron transmission measurements with the JEN-3 gauge. The neutron attenuation behavior of homogeneous and heterogeneous boron-alloyed steels was analyzed by increasing the material thickness gradually. As shown in Fig. 12, the simulations of micro-structure and homogeneous boron distribution within the steel plates yield approximately the same neutron attenuation. It can be concluded that the micro-structure in the sheets has no effect for uncollimated neutron beams as it is the case in the JEN-3 gauge or in neutron moderators.

6. Conclusions

The JEN-3 gauge, which is portable and also applicable for large sheets, offers a reliable inspection of neutron attenuation in boron-alloyed stainless steel-sheets in a thermal neutron field. This gauge using uncollimated neutron beam is well-suited to the investigation of attenuation character of shielding materials even if a localization of micro-structure in the investigated sample is not possible. More structural information can be gained with neutron radiography utilizing collimated beams. Performing NR measurements with well-defined reference plates at different neutron radiography stations allows to compare the facilities and to show the influence of the energy spectrum on the neutron attenuation in the boron-alloyed steels. The micro-structure and the beam hardening effect strongly influence the neutron attenuation of a strong absorbing material. Using ^{10}B isotope enriched boron-alloyed stainless steel sheets is favorable if considering the beam-hardening effect in thick samples. We applied a simple MCNP model (channel model) for the micro-structure as a first step to discriminate dominant transmission enhancing factors on the experimental results. A rough micro-structure level of the boron distribution has been derived. The specification of a more realistic random distribution of Ferro-borides as MCNP input is not readily done. A refined structural model for the absorber distribution including other strong materials like Gd in a steel and Al matrix will be subject to future investigations.

Acknowledgements

The authors would like to thank Burkhard Schillinger and Florian Gruenauer for helpful discussions, Peter Vontobel for the technical support during the experiments at NEUTRA-PSI. This work has financially been

supported by the EURATOM-OEAW (UT4 Project), and Böehler-Bleche GmbH, Muerzzuschlag, Austria.

References

[1] V.F. Sears, Neutron scattering lengths and cross-sections, Neutron News 3 (3) (1992) 26.
[2] J.C. Domanus, Practical Neutron Radiography, Kluwer, Netherlands, 1992.
[3] K.O. Vilpponen, A.E. Salmela, Scand. J. Metall. (Stockholm) 2 (1974) 298.
[4] Böhler-Bleche GmbH, Sheet and Plate for Nuclear Engineering, Böhler NEUTRONIT Archives, AV4/0281/77 (1997), and BBG/T/Dr.K/August 2001. Available from: <http://www.bohler-bleche.at>.
[5] J.F. Briesmeister, MCNP^{TM} – A General Monte Carlo N-Particle Transport Code, vols. 1–4, Version 4b.
[6] C.J. Leliveld, A fast Monte Carlo simulator for scattering in X-ray computerized tomography, Thesis, Zurich, Switzerland, 1996.
[7] M. Bastürk, Material inspections with low energy neutrons and 3D image reconstruction, Thesis, TU-Vienna, Austria, 2003.
[8] IAEA Nuclear Data Service. Available from: <http://www-nds.iaea.or.at/>.
[9] M. Zawisky, M. Bastürk, R. Derntl, F. Dubus, E. Lehmann, P. Vontobel, J. Appl. Radiat. Isotopes 61 (2004) 517.
[10] S. Körner, Digital image processing in neutron radiography, Thesis, TU-Vienna, 2000.
[11] B. Schillinger, Neue Entwicklungen zur Radiographie und Tomographie mit thermischen Neutronen und zu deren routinemäßigem Einsatz, Dissertation TU Munich, Mensch & Buch Verlag, Berlin, 1999.
[12] M. Zawisky, M. Bastürk, J. Rehacek, Z. Hradil, J. Nucl. Mater. 327 (2004) 188.
[13] N. Kardjilov, Further developments and applications of radiography and tomography with thermal and cold neutrons, Thesis, TU-Munich, Germany 2003. Available from: <tumb1.biblio.tu-muenchen.de/publ/diss/ph/2003/kardjilov.pdf>.